Ponencia presentada en SAAEI 2023, Sevilla 5-7 julio 2023

Modelling and simulation of dual three-phase PMSMs on the phase variable reference frame

Adriano Navarro-Temoche[1], Iñigo Kortabarria[1], Edorta Ibarra[1], Andrés Sierra-González[2]
[1]Departamento de Tecnología Electrónica, Universidad del País Vasco/Euskal Herriko Unibertsitatea (UPV/EHU)
[2]TECNALIA, Basque Research and Technology Alliance (BRTA)
adrianorai.navarro@ehu.eus

***Abstract*—In this paper, a per-phase model of a dual three-phase Permanent Magnet Synchronous Machine (PMSM) is mathematically developed and implemented in Simscape. This model provides accuracy and adaptability to easily represent machine operation under a number of phenomena such as open-phase faults, magnetic saturation, etc. Simulation results that show the correctness of the modelling approach are finally provided.**

***Index Terms*—PMSM, EV, phase variables, Simscape**

I. Introduction

Multi-phase machines are receiving a great attention as, compared to three-phase systems, they provide a reduced torque ripple, low harmonic content and an improved fault tolerance [1]–[4]. The six-phase configuration is one of the most studied of the multi-phase architectures. Depending on the phase arrangement between the three-phase sets, they can be classified into symmetrical (shifted by 0 or $\pi/3$) [5]–[7] or asymmetrical (shifted by $\pi/6$) [8]–[10]. With the asymmetrical configuration, the sixth harmonic torque pulsations produced by the two three-phase sets are in anti-phase and, therefore, they are cancelled [11]. Regarding their industrialisation, dual three-phase permanent magnet synchronous machines (PMSMs) have been successfully used in a variety of industry applications [12]–[17]. Among them, the automotive sector represents a highly demanding application, requiring operation for a very wide speed range and high torque [15]–[17].

In [18], several topologies of multiphase converters are discussed. Fig. 1 shows the most common arrangement of a dual three-phase system, where two voltage source inverters (VSI) share a common DC-link and feed two three-phase sets with isolated neutral points. Hereinafter, the first three-phase set will be named ABC, while the second will be named RST.

Simulation is a powerful tool for developing modern power systems. However, in order to carry out an in-depth and accurate analysis of the dual three-phase system in a variety of scenarios such as sensorless control, open-phase faults, and flux weakening operation, it is convenient to represent the machine as realistically as possible. Decoupled models with multiple vector spaces are commonly used to describe the behaviour of machines [19], [20]. Thus, despite these models allow the simulation of the normal operation of the machine, as well as easing the control implementation, they possess some drawbacks. For instance, machines using the decoupled model in open-phase fault scenarios have to be particularised (i.e. modify the vector transformations) depending on the phase(s) in fault [21], [22].

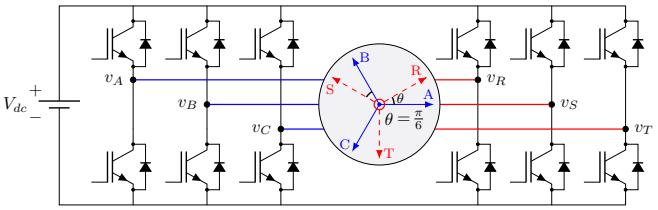

Fig. 1: Asymmetrical dual three-phase PMSM drive system.

In this paper, a simulation model is presented with the machine modelled in phase variables in Matlab/Simulink and using the Simscape library, as electrical elements can be customised, obtaining a more comprehensive model. To do so, the machine equations are rewritten from the parameters provided by the decoupled model used in the control strategy.

II. Mathematical modelling of dual three-phase PMSMs in phase variables

In a dual three-phase PMSM, the voltages across the stator windings are defined by

$$\mathbf{v}_s = \mathbf{R}\mathbf{i}_s + \frac{d\psi_s}{dt}, \tag{1}$$

where

$$\begin{aligned} \mathbf{R} &= R_s \mathbb{I}_n, \\ \mathbf{v}_s &= \begin{bmatrix} v_A & v_B & v_C & v_R & v_S & v_T \end{bmatrix}^T, \\ \mathbf{i}_s &= \begin{bmatrix} i_A & i_B & i_C & i_R & i_S & i_T \end{bmatrix}^T, \\ \psi_s &= \begin{bmatrix} \psi_A & \psi_B & \psi_C & \psi_R & \psi_S & \psi_T \end{bmatrix}^T, \end{aligned} \tag{2}$$

and $\{\mathbf{v}_s, \mathbf{i}_s, \psi_s\} \in \mathbb{R}^{6\times 1}$ are the voltage, current and stator flux vectors, respectively. The resistance matrix $\mathbf{R} \in \mathbb{R}^{6\times 6}$ is a diagonal matrix with its elements equal to the stator resistance R_s.

Phase stator flux and current vectors are linked by the stator inductance matrix $\mathbf{L}_s$ which, for salient-pole machines, is a function of the electrical rotor position θ_e (N_p times the mechanical position θ_m, where N_p is the number of pole-pairs of the machine):

$$\boldsymbol{\psi}_s(\theta_e) = \mathbf{L}_s(\theta_e)\mathbf{i}_s + \boldsymbol{\psi}_{PM}(\theta_e). \tag{3}$$

$\boldsymbol{\psi}_{PM} \in \mathbb{R}^{6\times 1}$ is the magnetic flux produced by the permanent magnets. The permanent magnet flux linking winding A is assumed at maximum when $\theta_e = 0$ and zero when $\theta_e = \pi/2$, and is defined as

$$\boldsymbol{\psi}_{PM}(\theta_e) = \lambda_m \begin{bmatrix} \cos(\theta_e) \\ \cos(\theta_e - 2\pi/3) \\ \cos(\theta_e + 2\pi/3) \\ \cos(\theta_e - \pi/6) \\ \cos(\theta_e - 5\pi/6) \\ \cos(\theta_e + \pi/2) \end{bmatrix}, \tag{4}$$

where λ_m is the maximum flux linkage of a phase, only produced by the permanent magnets, and it depends on the magnet properties and motor structure.

Thus, voltage equations are expressed as:

$$\mathbf{v}_s = \mathbf{R}\mathbf{i}_s + \frac{d\mathbf{L}_s(\theta_e)}{dt}\mathbf{i}_s + \mathbf{L}_s(\theta_e)\frac{d\mathbf{i}_s}{dt} + \frac{d\boldsymbol{\psi}_{PM}(\theta_e)}{dt}. \tag{5}$$

A. Inductance Modelling of Dual Three-Phase PMSMs

According to [23], assuming that eddy current and hysteresis losses, saturation, the harmonic components in self-inductances and mutual inductances with orders higher than second order can be neglected, and that the induced back-electromotive force (BEMF) is sinusoidal, the self-inductance L_{PP} can be expressed as:

$$L_{PP}(\theta_e) = L_{sl} + \bar{L}_{dqa} + \bar{L}_{dqd}\cos(2\theta_P), \tag{6}$$

where $\bar{L}_{dqa} = (\bar{L}_d + \bar{L}_q)/2$, $\bar{L}_{dqd} = (\bar{L}_d - \bar{L}_q)/2$, L_{sl} is the phase leakage inductance, $(L_{sl} + \bar{L}_d)$ and $(L_{sl} + \bar{L}_q)$ are the phase self-inductances when the phase winding axis are aligned with d-axis and q-axis of the PM rotor, respectively. The mutual inductance between phases in the same star winding can be expressed as:

$$M_{PQ}(\theta_e) = M_{dqa}\cos(\theta_P - \theta_Q) + M_{dqd}\cos(\theta_P + \theta_Q), \tag{7}$$

where P $\in \{A, B, C, R, S, T\}$, while Q stands for another phase, i.e. $P \neq Q$.

The mutual inductance between phases in different winding sets can be expressed as:

$$M_{12}(\theta_e) = M_{dq12a}\cos(\theta_1 - \theta_2) + M_{dq12d}\cos(\theta_1 + \theta_2). \tag{8}$$

where "1" and "2" subscript stand for a phase in the ABC winding set and RST winding set, respectively. M_{dqa} and M_{dqd} are the gains of DC and second harmonic components in the mutual inductances between phases in each set. M_{dq12a} and M_{dq12d} are the gains of DC and second harmonic components in the mutual inductances between phases in different winding sets.

Therefore, the whole 6×6 stator inductance matrix $\mathbf{L}_s(\theta_e)$ consists of four 3×3 inductance matrices. The upper left $\mathbf{L}_1(\theta_e)$ and lower right $\mathbf{L}_2(\theta_e)$ matrices contain the $L_{PP}(\theta_e)$ and $M_{PQ}(\theta_e)$ coefficients defined by (6) and (7), and are related to the first and the second winding set, respectively. The upper right matrix $\mathbf{M}_{12}(\theta)$ and its transpose $\mathbf{M}_{21}(\theta_e) = \mathbf{M}_{12}^T(\theta_e)$ in the lower left are related to the mutual coupling between different sets defined by (8). Thus, the whole inductance matrix for the stator windings can be represented as a block matrix:

$$\mathbf{L}_s(\theta_e) = \begin{bmatrix} \mathbf{L}_1(\theta_e) & \mathbf{M}_{12}(\theta_e) \\ \mathbf{M}_{21}(\theta_e) & \mathbf{L}_2(\theta_e) \end{bmatrix}, \tag{9}$$

where the submatrices are given by

$$\mathbf{L}_1(\theta_e) = \begin{bmatrix} L_{AA}(\theta_e) & M_{AB}(\theta_e) & M_{AC}(\theta_e) \\ M_{BA}(\theta_e) & L_{BB}(\theta_e) & M_{BC}(\theta_e) \\ M_{CA}(\theta_e) & M_{CB}(\theta_e) & L_{CC}(\theta_e) \end{bmatrix}, \tag{10a}$$

$$\mathbf{L}_2(\theta_e) = \begin{bmatrix} L_{RR}(\theta_e) & M_{RS}(\theta_e) & M_{RT}(\theta_e) \\ M_{SR}(\theta_e) & L_{SS}(\theta_e) & M_{ST}(\theta_e) \\ M_{TR}(\theta_e) & M_{TS}(\theta_e) & L_{TT}(\theta_e) \end{bmatrix}, \tag{10b}$$

$$\mathbf{M}_{12}(\theta_e) = \begin{bmatrix} M_{AR}(\theta_e) & M_{AS}(\theta_e) & M_{AT}(\theta_e) \\ M_{BR}(\theta_e) & M_{BS}(\theta_e) & M_{BT}(\theta_e) \\ M_{CR}(\theta_e) & M_{CS}(\theta_e) & M_{CT}(\theta_e) \end{bmatrix}. \tag{10c}$$

Once the dynamic model that relates voltages and currents is defined, the electromagnetic torque (T_e) produced by the motor is need to be found. To do so, the magnetic coenergy W_{co} can be expressed as [24]:

$$W_{co} = \frac{1}{2}\mathbf{i}_s^T\mathbf{L}_s\mathbf{i}_s + \mathbf{i}_s^T\boldsymbol{\psi}_{PM}. \tag{11}$$

Hence, the electromagnetic torque expression, obtained by differentiating the magnetic coenergy with respect to the mechanical rotor position θ_m, is:

$$T_e = N_p\left(\frac{1}{2}\mathbf{i}_s^T\frac{d\mathbf{L}_s}{d\theta_e}\mathbf{i}_s + \mathbf{i}_s^T\frac{d\boldsymbol{\psi}_{PM}}{d\theta_e}\right). \tag{12}$$

The first term of (12) is related to the reluctance torque, whereas the second one corresponds to the magnetic torque. When SPMSMs are used, the former will be zero as, for non-salient machines, $\mathbf{L}_s$ is constant with respect to θ_e.

B. Model represented in dq-reference frame

To ease the control of the six-dimensional machine system, according to the vector space decomposition (VSD) theory [25], the machine can be decomposed into three orthogonal sub-spaces, i.e. $\alpha\beta$, XY and o_1o_2. By applying the transformation matrix T_6, harmonics are mapped to different sub-planes, as shown in Table I.

TABLE I: Harmonic decomposition using VSD model.

Sub-space	Harmonics	h
$\alpha\beta$	Fund. and $(12k \pm 1) \Rightarrow k = 1, 2, 3, \ldots$	$1, 11, 13, \ldots$
XY	$(6k \pm 1) \Rightarrow k = 1, 3, 5, \ldots$	$5, 7, 17, 19, \ldots$
o_1o_2	$(3k) \Rightarrow k = 1, 3, 5, \ldots$	$3, 9, 15, 21, \ldots$

$$\begin{aligned} &\begin{bmatrix} F_\alpha & F_\beta & F_X & F_Y & F_{o_1} & F_{o_2} \end{bmatrix}^T = \\ &= \mathbf{T}_6 \cdot \begin{bmatrix} F_A & F_B & F_C & F_R & F_S & F_T \end{bmatrix}^T, \end{aligned} \tag{13}$$

$$\mathbf{T}_6 = \frac{1}{3}\begin{bmatrix} 1 & \cos(4\theta_s) & \cos(8\theta_s) & \cos(\theta_s) & \cos(5\theta_s) & \cos(9\theta_s) \\ 0 & \sin(4\theta_s) & \sin(8\theta_s) & \sin(\theta_s) & \sin(5\theta_s) & \sin(9\theta_s) \\ 1 & \cos(8\theta_s) & \cos(4\theta_s) & \cos(5\theta_s) & \cos(\theta_s) & \cos(9\theta_s) \\ 0 & \sin(8\theta_s) & \sin(4\theta_s) & \sin(5\theta_s) & \sin(\theta_s) & \sin(9\theta_s) \\ 1 & 1 & 1 & 0 & 0 & 0 \\ 0 & 0 & 0 & 1 & 1 & 1 \end{bmatrix},$$

where $\theta_s = \pi/6$.

By applying the standard Park transformation, the variables in $\alpha\beta$ sub-plane can be converted to the synchronous dq-frame for a dual three-phase system.

$$\begin{bmatrix} F_d \\ F_q \end{bmatrix} = \underbrace{\begin{bmatrix} \cos\theta & \sin\theta \\ -\sin\theta & \cos\theta \end{bmatrix}}_{T_{dq}} \begin{bmatrix} F_\alpha \\ F_\beta \end{bmatrix}. \tag{14}$$

In addition, according to [26], the variables in the XY sub-plane can be converted to a new frame designated as xy-frame by applying the following transformation

$$\begin{bmatrix} F_x \\ F_y \end{bmatrix} = \underbrace{\begin{bmatrix} -\cos\theta & \sin\theta \\ \sin\theta & \cos\theta \end{bmatrix}}_{T_{xy}} \begin{bmatrix} F_X \\ F_Y \end{bmatrix}, \tag{15}$$

where F is V, I or ψ, which correspond to voltage, current and flux, respectively. Then, the harmonics in the XY sub-plane are converted into $(6k)$th harmonics in the xy-frame.

It is worth noting that the third sub-plane o_1o_2 cannot be exploited (i.e., open circuit) as the neutral points of the each three-phase set are isolated and are not connected between them. Hence, $I_{o_1} = I_{o_2} = 0$.

Thus, the resulting rotating transformation $\mathbf{T}_{\text{rot}}$ is defined as

$$\mathbf{T}_{\text{rot}} = \begin{bmatrix} \mathbf{T}_{dq} & \mathbf{0_2} & \mathbf{0_2} \\ \mathbf{0_2} & \mathbf{T}_{xy} & \mathbf{0_2} \\ \mathbf{0_2} & \mathbf{0_2} & \mathbf{I_2} \end{bmatrix} \mathbf{T}_6, \tag{16}$$

and the inductance matrix $\mathbf{L}_{dqxy}$, which does not consider the zero-sequence subspace o_1o_2, can be obtained from (9) as

$$\mathbf{L}_{dqxy} = \mathbf{T}_{\text{rot}}\mathbf{L}_s(\theta_e)\mathbf{T}_{\text{rot}}^{-1} = \begin{bmatrix} L_d & 0 & 0 & 0 \\ 0 & L_q & 0 & 0 \\ 0 & 0 & L_x & 0 \\ 0 & 0 & 0 & L_y \end{bmatrix}, \tag{17}$$

where

$$L_d = L_{sl} + 3\bar{L}_d, \quad L_x = L_{sl}, \tag{18a}$$
$$L_q = L_{sl} + 3\bar{L}_q, \quad L_y = L_{sl}. \tag{18b}$$

Therefore, the voltage equations in the dq-frame and xy-frame can be expressed as

$$\begin{aligned} \begin{bmatrix} V_d \\ V_q \end{bmatrix} &= \begin{bmatrix} R_s + L_d s & 0 \\ 0 & R_s + L_q s \end{bmatrix} \begin{bmatrix} I_d \\ I_q \end{bmatrix} + \omega_e \begin{bmatrix} -L_q I_q \\ L_d I_d + \lambda_m \end{bmatrix}, \\ \begin{bmatrix} V_x \\ V_y \end{bmatrix} &= \begin{bmatrix} R_s + L_x s & 0 \\ 0 & R_s + L_y s \end{bmatrix} \begin{bmatrix} I_x \\ I_y \end{bmatrix} + \omega_e \begin{bmatrix} -L_y I_y \\ L_x I_x \end{bmatrix}, \end{aligned} \tag{19}$$

Finally, the electromagnetic torque in the dq-frame is defined as

$$T_e = 3N_p(\lambda_m + (L_d - L_q)I_d)I_q. \tag{20}$$

III. Machine Model Implementation of the Phase Variable Model in Simscape

Using Simscape, it is possible to describe, in detail, the equivalent electrical circuit of the machine by coding each of the electrical elements. Owing to this, physical phenomena related to inductances, magnetic saturation, etc., can be incorporated into the model, enhancing the performance of the model.

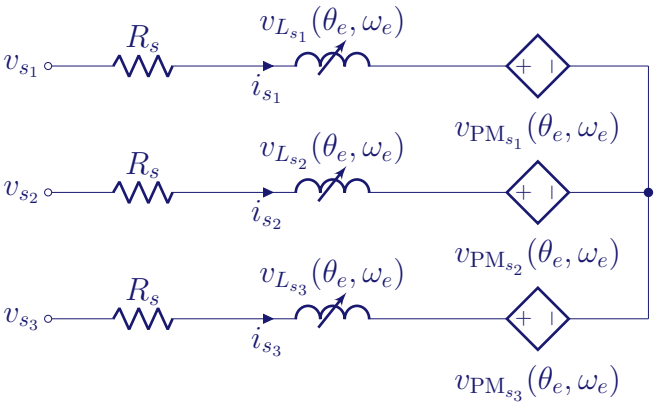

Fig. 2: Equivalent electrical circuit for each three-phase set $(s_1, s_2, s_3) = \{(A, B, C), (R, S, T)\}$ implemented using the Simscape library.

In this paper, the dual three-phase PMSM model in Simscape is carried out following the voltage equations for each three-phase set defined in (5). In Fig. 2, the electrical circuit for phase voltages is depicted, where each three-phase set is shown with its corresponding isolated neutral point. Thus, the main purpose is to rewrite the voltage terms in (5) in function of variables provided by the VSD model.

With respect to the voltage term $d\boldsymbol{\psi}_{PM}(\theta_e)/dt$ in (5) associated with the BEMF, it can be redefined as follows

$$v_{\text{PM}_s}(\theta_e, \omega_e) = \omega_e \tfrac{d\boldsymbol{\psi}_{PM}(\theta_e)}{d\theta_e} = -\omega_e \lambda_m \begin{bmatrix} \sin(\theta_e) \\ \sin(\theta_e - 2\pi/3) \\ \sin(\theta_e + 2\pi/3) \\ \sin(\theta_e - \pi/6) \\ \sin(\theta_e - 5\pi/6) \\ \sin(\theta_e + \pi/2) \end{bmatrix}. \tag{21}$$

From (21), it is concluded that v_{PM_s} is function of the electrical motor speed and position.

As for the voltage terms $\frac{d\mathbf{L}_s(\theta_e)}{dt}\mathbf{i}_s + \mathbf{L}_s(\theta_e)\frac{d\mathbf{i}_s}{dt}$ in (5), related to the inductance matrix defined in (9), these terms can be rewritten using $\mathbf{L}_{dqxy}$ from the VSD model. Thus, (9) can be expressed in terms of $\mathbf{L}_{dqxy}$ as

$$\mathbf{L}_s(\theta_e) = \mathbf{T}_{\text{rot}}^{-1}\mathbf{L}_{dqxy}\mathbf{T}_{\text{rot}}, \tag{22}$$

and, the time derivative of (9) is:

$$\begin{aligned} \frac{d\mathbf{L}_s(\theta_e)}{dt} &= \omega_e \frac{d\mathbf{L}_s(\theta_e)}{d\theta_e} = \omega_e \frac{d(\mathbf{T}_{\text{rot}}^{-1}\mathbf{L}_{dqxy}\mathbf{T}_{\text{rot}})}{d\theta_e} = \\ &= \omega_e \left(\frac{d\mathbf{T}_{\text{rot}}^{-1}}{d\theta_e}\mathbf{L}_{dqxy}\mathbf{T}_{\text{rot}} + \mathbf{T}_{\text{rot}}^{-1}\mathbf{L}_{dqxy}\frac{d\mathbf{T}_{\text{rot}}}{d\theta_e} \right). \end{aligned} \tag{23}$$

Therefore, voltage equations for the Simscape integration can be expressed as

$$\mathbf{v}_s = \mathbf{R}\mathbf{i}_s + v_{L_s}(\theta_e, \omega_e) + v_{\text{PM}_s}(\theta_e, \omega_e), \tag{24}$$

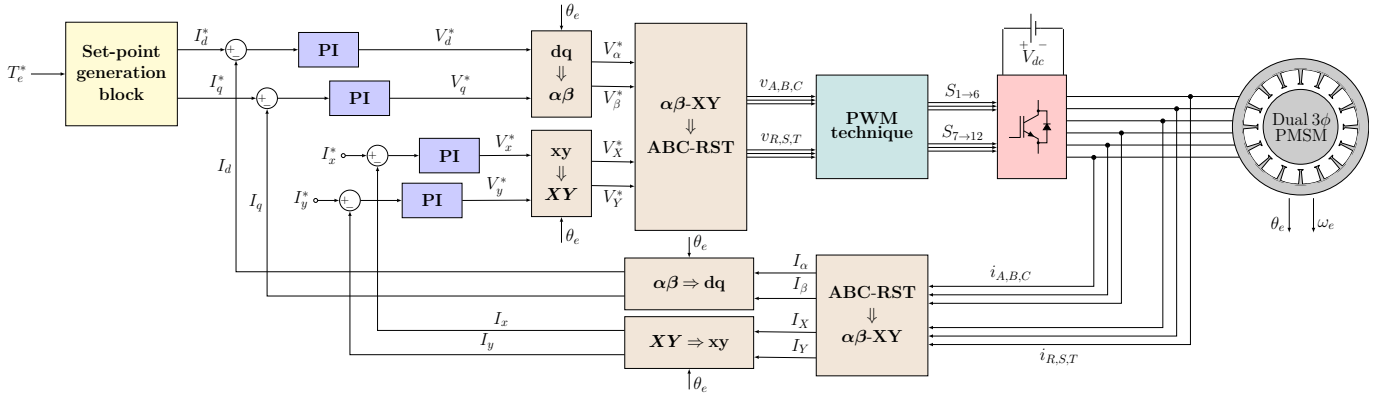

Fig. 3: FOC structure for dual three-phase machines following the VSD representation.

where $s = \{A, B, C, R, S, T\}$ and,

$$v_{L_s}(\theta_e, \omega_e) = \frac{d\mathbf{L}_s(\theta_e)}{dt}\mathbf{i}_s + \mathbf{L}_s(\theta_e)\frac{d\mathbf{i}_s}{dt} = \\ = \omega_e \left(\frac{d\mathbf{T}_{\text{rot}}^{-1}}{d\theta_e}\mathbf{L}_{dqxy}\mathbf{T}_{\text{rot}} + \mathbf{T}_{\text{rot}}^{-1}\mathbf{L}_{dqxy}\frac{d\mathbf{T}_{\text{rot}}}{d\theta_e} \right) \mathbf{i}_s \\ + (\mathbf{T}_{\text{rot}}^{-1}\mathbf{L}_{dqxy}\mathbf{T}_{\text{rot}})\frac{d\mathbf{i}_s}{dt}. \tag{25}$$

On the other hand, the electromagnetic torque can be rewritten by replacing (22) into (12) as

$$T_e = N_p \left(\frac{1}{2}\mathbf{i}_s^T \frac{d(\mathbf{T}_{\text{rot}}^{-1}\mathbf{L}_{dqxy}\mathbf{T}_{\text{rot}})}{d\theta_e}\mathbf{i}_s + \mathbf{i}_s^T \frac{d\boldsymbol{\psi}_{PM}(\theta_e)}{d\theta_e} \right). \tag{26}$$

Finally, regarding magnetic saturation, this phenomenon can be simply taken into account in this Simscape model by inserting Look-Up Tables (LUTs) for the inductances (L_d,L_q,L_{sl}) and permanent magnet flux (λ_m) in terms of the currents in dq-frame, and for the stator resistance R_s in terms of the temperature.

A. Description of the implemented Field oriented control

Once modelled the PMSM in phase variables, Fig. 3 shows how the machine is controlled with a Field Oriented Control (FOC) approach by using the VSD model developed in Section II-B.

With respect to the control strategy, for a given reference torque, a reference current pair in the dq-frame (I_d^*, I_q^*) is generated. Furthermore, in healthy situation, currents in the no-torque frame (i.e. xy) (I_x^*, I_y^*) are usually set to 0 for machines with sinusoidally distributed windings and, as the neutral points of the two three-phase sets are isolated and are not connected in this application, currents in the o_1o_2 sub-space are zero. In addition, a PWM with 3rd harmonic injection, which pulses are sent to the two three-phase VSIs, is used.

Up to nominal speed, the current references I_d^* and I_q^* are generated to be referred to the Maximum Torque per Ampere (MTPA) curve, which guarantees minimum copper losses [27]. To extend the operating speed range of this EV drive, for speeds beyond the nominal one, a set-point generator block considering Flux Weakening (FW) region is included.

TABLE II: Parameters of the dual three-phase IPMSM drive.

Parameter	Value	Parameter	Value
Number of pole pairs N_p	19	Stator resistance R_s	61.43 [$m\Omega$]
d-axis inductance L_d	1.00 [mH]	q-axis inductance L_q	1.35 [mH]
Leakage inductance L_{sl}	0.9 [mH]	PM flux linkage λ_m	0.038 [Wb]
DC bus nominal voltage V_{dc}	400 [V]	Maximum torque T_{max}	54 [N.m]
Maximum mech. speed ω_m	5000 [rpm]	Switching frequency f_{sw}	25 [kHz]
Simulation step T_s	1 [μs]		

IV. Simulation results

As stated before, a detailed model of an asymmetrical dual three-phase IPMSM drive, whose most relevant parameters are listed in Table II, has been implemented in the Matlab/Simulink environment using the Simscape library together with its control.

In Fig. 4, the spatial distribution of the self-inductance L_{AA} and mutual inductances in phase A are shown. These values are quite similar to those obtained in prototypes found in the literature [28]. In this application, mutual inductances are much smaller than the self-inductance; however, depending on the cross-coupling between each phase and each three-phase set, these can be significant.

The first simulation test consists in referring the system to an MTPA point with a mechanical speed equal to 200 [rpm] and a reference torque equal to 22 [N.m] in order to analyse its response. In this operating point, without loss of generality, the phase A enters in fault at 3.2 [ms]. Thus, the currents of the first three-phase set (ABC) are shown, before and after the fault, in Fig. 5. This proves that the model is capable of modifying its response easily in the presence of a fault without particularising the vector transformations.

On the other hand, in order to prove the performance of the model and its control, the system has been tested under close-to-real driving conditions. In particular, the torque and speed profiles have been calculated for a given EV which is circulating under the New European Driving Cycle (NEDC).

As aforementioned, a flux weakening control is included in the current set-point generation block to test the response of

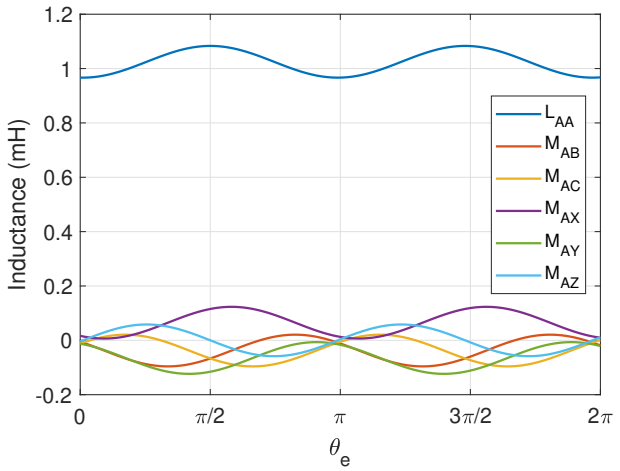

Fig. 4: Self-inductance and mutual inductances in phase A.

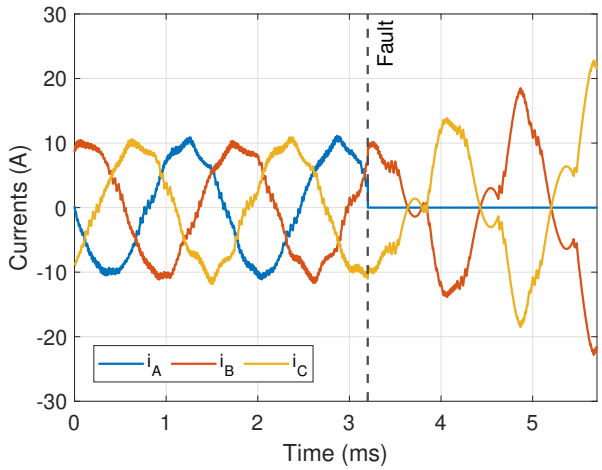

Fig. 5: Phase currents tested under fault in phase A.

the motor model at high speeds. Thus, the presented simulations only focus on the extra-urban driving profile interval of the NEDC as here, the motor enters in flux weakening region. As shown in Fig. 6, the flux weakening control works correctly as the voltage utilisation is limited to the voltage constraint (dashed line in Fig. 6a) and the dq-currents are also limited to the maximum current curve (dashed line in Fig. 6b), even when the motor speed increases beyond nominal values. With these results, it is demonstrated that the motor model is well-integrated with the control board and it can provide proper measurements such as phase currents, rotor position, and rotor speed.

Finally, regarding the torque provided by the machine, it is calculated by means of (26) which considers the whole 6x6 inductance matrix (9). Thus, in Fig. 7, it is shown that the interior PMSM is correctly represented as not only its torque follows the reference properly throughout the driving cycle but also it is similar to the torque in dq-frame calculated by (20).

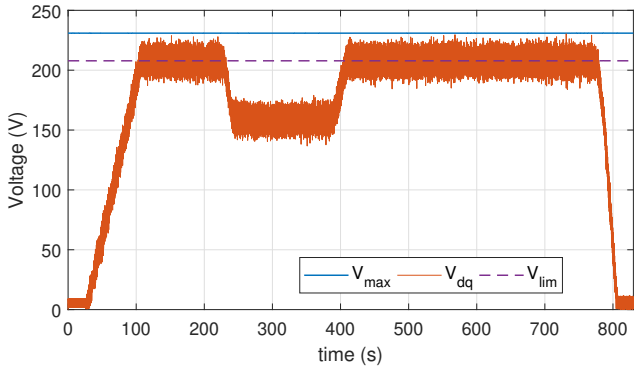

(a) Voltage utilisation considering the FW operating region.

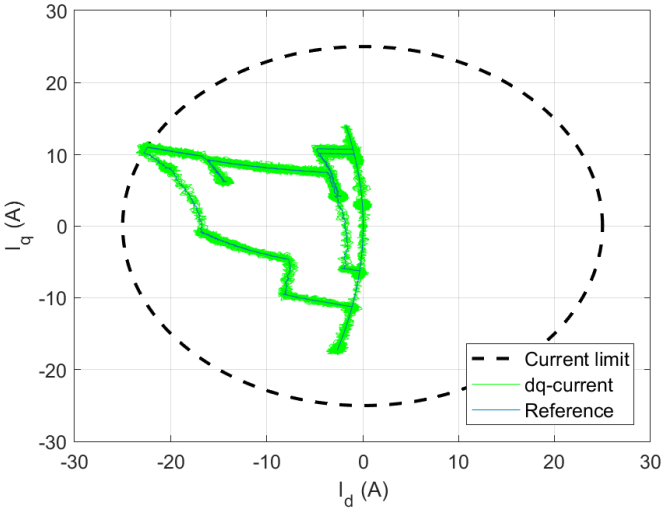

(b) Current loci in the dq-frame

Fig. 6: Flux Weakening Control results.

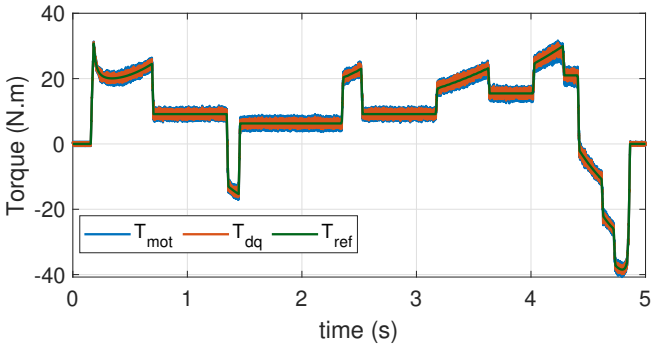

Fig. 7: Electromagnetic torque (green: reference, red: from (20), blue: from motor in phase variables) throughout NEDC

V. Conclusions

In this work, a Simscape representation for dual three-phase PMSMs is modelled in phase variables. Using this model, a better understanding of the performance in each phase can be analysed depending on the case study.

Furthermore, owing to the use of Simscape library, the

adaptability of the proposed motor model is the main advantage using this approach, open-phase faults, neutral point configurations and magnetic saturation can be easily taken into account. Thus, a more comprehensive model is obtained. However, it should be borne in mind that, the more complexity is added to the motor model, the more computational burden it will have.

The model can be used to represent for PMSM both with interior and with surface-mounted permanent magnets. It should be noted that calculations are greatly reduced when a SPMSM is used as the inductance matrix does not vary with respect to the electrical position.

Finally, despite this motor model is tested using a FOC, any control strategy can be applied over the model such as Direct Torque Control, Model Predictive Control or Combined Control.

ACKNOWLEDGEMENTS

This work was supported in part by the Government of the Basque Country within the fund for research groups of the Basque University system IT1440-22 and by the MCIN/AEI/10.13039/501100011033 within the project PID2020-115126RB-I00.

REFERENCES

[1] P. Wang, S. Gong, X. Sun, Z. Liu, D. Jiang, and R. Qu, "Fault-tolerant reconfiguration topology and control strategy for symmetric open-winding multiphase machines," *IEEE Transactions on Industrial Electronics*, vol. 69, no. 9, pp. 8656–8666, 2022.

[2] A. G. Yepes, W. E. Abdel-Azim, A. Shawier, M. S. Abdel-Majeed, H. S. Che, A. S. Abdel-Khalik, S. Ahmed, and J. Doval-Gandoy, "Online control strategy for tolerating resistance asymmetry with minimum copper loss in the full torque range for symmetrical six-phase ac drives," *IEEE Transactions on Power Electronics*, vol. 38, no. 1, pp. 151–164, 2023.

[3] A. G. Yepes, O. Lopez, I. Gonzalez-Prieto, M. J. Duran, and J. Doval-Gandoy, "A comprehensive survey on fault tolerance in multiphase ac drives, part 1: General overview considering multiple fault types," *Machines*, vol. 10, no. 3, 2022.

[4] A. G. Yepes, I. Gonzalez-Prieto, O. Lopez, M. J. Duran, and J. Doval-Gandoy, "A comprehensive survey on fault tolerance in multiphase ac drives, part 2: Phase and switch open-circuit faults," *Machines*, vol. 10, no. 3, 2022.

[5] H. S. Che and W. P. Hew, "Dual three-phase operation of single neutral symmetrical six-phase machine for improved performance," in *Proceedings of 41st Annual Conference of the IEEE Industrial Electronics Society (IECON)*, pp. 001176–001181, 2015.

[6] Z. Liang, D. Liang, P. Kou, and Q. Ze, "Modeling and bumpless switching control of symmetrical dual three-phase PMSM in two operating modes," *Electric Power Components and Systems*, vol. 48, no. 3, pp. 304–319, 2020.

[7] Z. Liang, D. Liang, P. Kou, and S. Jia, "Postfault control and harmonic current suppression for a symmetrical dual three-phase spmsm drive under single-phase open-circuit fault," *IEEE Access*, vol. 8, pp. 67674–67686, 2020.

[8] Y. Luo and C. Liu, "A simplified model predictive control for a dual three-phase PMSM with reduced harmonic currents," *IEEE Transactions on Industrial Electronics*, vol. 65, pp. 9079–9089, nov 2018.

[9] C. Zhou, G. Yang, and J. Su, "PWM strategy with minimum harmonic distortion for dual three-phase permanent-magnet synchronous motor drives operating in the overmodulation region," *IEEE Transactions on Power Electronics*, vol. 31, no. 2, pp. 1367–1380, 2016.

[10] Z. Shen, D. Jiang, Z. Liu, D. Ye, and J. Li, "Common-mode voltage elimination for dual two-level inverter-fed asymmetrical six-phase pmsm," *IEEE Transactions on Power Electronics*, vol. 35, no. 4, pp. 3828–3840, 2020.

[11] K. Gopakumar, S. Sathiakumar, S. Biswas, and J. Vithayathil, "Modified current source inverter fed induction motor drive with reduced torque pulsations," *IEE Proceedings B Electric Power Applications*, vol. 131, pp. 159–164(5), July 1984.

[12] S. Hu, Z. Liang, W. Zhang, and X. He, "Research on the integration of hybrid energy storage system and dual three-phase PMSM drive in EV," *IEEE Transactions on Industrial Electronics*, vol. 65, no. 8, pp. 6602–6611, 2018.

[13] J. Xu, B. Zhang, H. Fang, and H. Guo, "Guaranteeing the fault transient performance of aerospace multiphase permanent magnet motor system: An adaptive robust speed control approach," *CES Transactions on Electrical Machines and Systems*, vol. 4, no. 2, pp. 114–122, 2020.

[14] Y. Xiao, C. Liu, and F. Yu, "An effective charging-torque elimination method for six-phase integrated on-board ev chargers," *IEEE Transactions on Power Electronics*, vol. 35, no. 3, pp. 2776–2786, 2020.

[15] A. Salem and M. Narimani, "A review on multiphase drives for automotive traction applications," *IEEE Transactions on Transportation Electrification*, vol. 5, no. 4, pp. 1329–1348, 2019.

[16] S. V. Nair, H. P., and K. Hatua, "Six-step operation of a symmetric dual three-phase pmsm with minimal circulating currents for extended speed range in electric vehicles," *IEEE Transactions on Industrial Electronics*, vol. 69, no. 8, pp. 7651–7662, 2022.

[17] S. V. Nair, K. Layek, and K. Hatua, "An unequal split dual three-phase pmsm with extended torque-speed characteristics for automotive application," *IEEE Transactions on Power Electronics*, vol. 37, no. 10, pp. 12437–12449, 2022.

[18] Z. Liu, Y. Li, and Z. Zheng, "A review of drive techniques for multiphase machines," *CES Transactions on Electrical Machines and Systems*, vol. 2, no. 2, pp. 243–251, 2018.

[19] A. Tessarolo, "Modeling and simulation of multiphase machines in the matlab/simulink environment," in *Engineering Education and Research Using MATLAB* (A. H. Assi, ed.), ch. 1, Rijeka: IntechOpen, 2011.

[20] E. Levi, "Multiphase AC machines," in *Power Electronics and Motor Drives*, ch. 3, pp. 1–30, CRC Press, 2016.

[21] Z. Changpan, T. Wei, S. Xiang dong, Z. Zhaoji, Y. Guijie, and S. Jianyong, "Control strategy for dual three-phase pmsm based on reduced order mathematical model under fault condition due to open phases," *The Journal of Engineering*, vol. 2018, no. 13, pp. 489–494, 2018.

[22] Y. Hu, Z. Q. Zhu, and Z.-y. Wu, "Modelling and vector control of dual three-phase pmsm with one-phase open," *IET Electric Power Applications*, vol. 15, no. 7, pp. 847–860, 2021.

[23] S. Kallio, M. Andriollo, A. Tortella, and J. Karttunen, "Decoupled d-q model of double-star interior-permanent-magnet synchronous machines," *IEEE Transactions on Industrial Electronics*, vol. 60, pp. 2486–2494, jun 2013.

[24] P. Krause, O. Wasynczuk, S. Sudhoff, and S. Pekarek, *Analysis of Electric Machinery and Drive Systems*. John Wiley & Sons, Inc., June 2013.

[25] Y. Zhao and T. Lipo, "Space vector PWM control of dual three-phase induction machine using vector space decomposition," *IEEE Transactions on Industry Applications*, vol. 31, no. 5, pp. 1100–1109, 1995.

[26] Y. Hu, Z. Q. Zhu, and K. Liu, "Current control for dual three-phase permanent magnet synchronous motors accounting for current unbalance and harmonics," *IEEE Journal of Emerging and Selected Topics in Power Electronics*, vol. 2, pp. 272–284, 2014.

[27] A. Dianov, F. Tinazzi, S. Calligaro, and S. Bolognani, "Review and classification of MTPA control algorithms for synchronous motors," *IEEE Transactions on Power Electronics*, vol. 37, no. 4, pp. 3990–4007, 2022.

[28] Y. Hu, Z. Q. Zhu, and M. Odavic, "Comparison of two-individual current control and vector space decomposition control for dual three-phase pmsm," *IEEE Transactions on Industry Applications*, vol. 53, no. 5, pp. 4483–4492, 2017.